Hydrogen Beta Index Calculation for Delta Scuti Variable Stars

Kelsey Jorgenson

A senior thesis submitted to the faculty of
Brigham Young University
in partial fulfillment of the requirements for the degree of

Bachelor of Science

Eric Hintz, Advisor

Department of Physics and Astronomy

Brigham Young University

April 2011

ABSTRACT

Hydrogen Beta Index Calculation for Delta Scuti Variable Stars

Kelsey Jorgenson
Department of Physics and Astronomy
Bachelor of Science

In this study I calculated the Hβ index values for a set of δ Scuti variable stars. The Hβ index is commonly used to measure surface temperature of stars as well as the age of stars or clusters. The survey contained known δ Scuti stars located in the northern hemisphere as well as a few additional well-known variable stars. This provided a sample of approximately 190 stars. Observations were made with the 1.2-m and 1.85-m telescopes at the Dominion Astrophysical Observatory. I present 68 previously unpublished Hβ indexes and compare these index values with other common temperature measurements of stars.

Keywords: observational astronomy, spectroscopy, variable stars, Delta Scuti stars

ACKNOWLEDGMENTS

Thank you to my family for supporting me in pursuing what I love, and to my research advisor Dr. Hintz for helping me through both the project and this thesis. Thank you to my Physics 416 professors, Dr. Ware and Dr. Van Huele, for giving me feedback and pressing me to improve my writing. Finally, thank you to my roommates, for putting up with me through this stressful process.

Contents

Chapter 1

Introduction

In this thesis I describe my research project of calculating hydrogen beta (Hβ) indexes for a set of δ Scuti variable stars. In the introduction I will explain the purpose of my research project, concepts that are useful to know for my thesis, including the magnitude system, interstellar reddening, stellar classification, and variable stars, as well as discuss the background of my research.

1.1 Purpose of the Research Project

The aim of this research project is to fill in information gaps in the catalogue of information of known δ Scuti stars. This is in the form of the Hβ index. Astronomical understanding is increased through observations and analysis of said observations; therefore more information about δ Scuti stars will help astronomers to characterize them more precisely. Other astronomers can use the information I have extracted as part of my research for their own research projects, draw patterns, and advance the field of astronomy.

1.2 The Magnitude System

Astronomers measure the brightness of celestial objects in terms of magnitudes. In the second century B.C. the Greek astronomer Hipparchus devised a brightness scale for stars based off of the brightness of stars that can be seen with the naked eye. He designated the brightest stars first magnitude and the dimmest stars sixth magnitude, with the rest falling between first and sixth magnitude. Astronomers continue to use the magnitude system, mainly out of tradition, and this system has been adapted for use today. In the modern scale, Vega has an apparent magnitude of 0.03, Polaris (the North Star) has an apparent magnitude of 1.97, and the Sun has an apparent magnitude of -26.74. Magnitudes are logarithmic units; this choice of units stems from the fact that the eye detects light on a logarithmic scale. The magnitude system also runs backwards. That is to say, a lower or more negative magnitude number signifies greater brightness or luminosity. There are two types of astronomical magnitudes: apparent magnitude and absolute magnitude. Apparent magnitude is related to the flux of an object by the following equation:

$$m - m_0 = -2.5 \log_{10} \frac{F}{F_0}$$

where m is the apparent magnitude of an object, F is its flux, in units of photons s^{-1} (counted by the detector), and m_0 and F_0 are the apparent magnitude and flux of an object of comparison. Absolute magnitude is an object's apparent magnitude if it were 10 parsecs away from the earth. This allows astronomers to compare the true brightnesses of objects independent of distance.

Magnitudes are generally calculated within a certain wavelength filter. These filters have a central wavelength and extend a certain width above and below the central wavelength. Frequently it is informative to take the difference of magnitudes in different filters of the same star. For instance, the Strömgren *b* filter is centered on 4670 Å with a half-width of 180 Å, while the Strömgren *y* filter is centered on 5470 Å with a half-width of 230 Å. Since the vast majority of a star's radiation is thermal in origin, taking the difference between a star's magnitude in its *b* and *y* filters (designated

b-y) can indicate a star's relative temperature. A lower *b-y* value indicates a star is hotter, while a higher value indicates the opposite. Quantities involving subtracting two magnitudes centered on different wavelengths are called color indexes.

1.3 Interstellar Reddening

Frequently we do not receive as much radiation from a star as we would expect. The reason behind this decreased radiation is extinction, and in particular, interstellar reddening. Extinction refers to the general absorption and scattering of electromagnetic radiation by matter that lies between the astronomical object and the observer. Reddening is a specific type of extinction wherein dust grains or particles with sizes on the order of 1 μm scatter or absorb radiation with wavelengths close to the size of the particle. This means that shorter or bluer wavelengths are scattered or absorbed more than longer, redder wavelengths. The effect of reddening is to make a celestial object appear more red than it is intrinsically. Reddening, and extinction in general, interferes with astronomers' ability to correctly classify stars.

1.4 Stellar Classification

Modern astronomy and the vast advancements in theoretical astronomical understanding that accompany it have come about largely thanks to accurate stellar classification. Stars are classified according to their spectral characteristics into spectral types. This taxonomy was developed in the early twentieth century by Harvard astronomer Edward C. Pickering, and two assistants (Carroll & Ostlie 2007). These scientists initially classified spectra by the strength of their hydrogen absorption lines, labeling them with capital letters starting at A and continuing onward. Later the classification scheme was changed to reflect increasing intrinsic stellar temperature rather than the strength of their hydrogen absorption lines. This changed the alphabetical spectral type sequence

to "O B A F G K M." The intermediate letters not present were absorbed in the letters given. The physical basis of the distinction of this spectral classification system comes from the electronic transitions of different atomic orbitals of elements and compounds in the atmospheres of these stars (Carroll & Ostlie 2007). The reason the hottest stars do not have the strongest hydrogen absorption lines is that at the temperatures of these stars, hydrogen is ionized and therefore no electronic transitions can occur in hydrogen orbitals.

1.5 The Hertzsprung-Russell Diagram

Once the Harvard classification was established, astronomers began to compare stars' spectral types with other quantities such as mass and absolute magnitude. Two astronomers, Ejnar Hertzsprung and Henry Norris Russell, independently compared the absolute values of stars with their spectral types and established the same correlation. They both also discovered that stars of type G had a range of magnitudes or brightnesses for each spectral type (Carroll & Ostlie 2007). They noted three main magnitude ranges for each spectral type starting at G and increasing with temperature. The upper branch of stars were dubbed giants and the lower branch of stars were designated dwarfs. This diagram, independently produced by both Hertzsprung and Russell, lead to the modern Hertzsprung-Russell (H-R) diagram. Ultimately, the H-R diagram plots stellar temperature vs. luminosity. There are several forms of the H-R diagram. For observational purposes, it is often convenient to plot absolute magnitude, a measure of intrinsic luminosity, and a color index such as *b-y*. This kind of H-R diagram is known as a color-magnitude diagram or CM diagram. Figures 1.1 and 1.2 are both examples of CM diagrams.

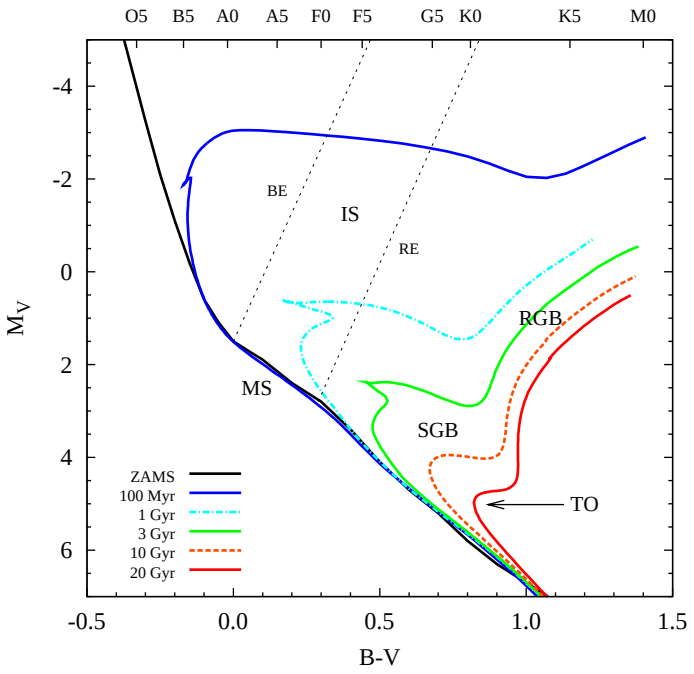

Figure 1.1 A CM diagram plotting absolute magnitude (M_V) vs. $B-V$. The different colored lines represent differing ages of stellar populations, starting from zero-age main sequence (ZAMS) populations. RGB stands for red giant branch; SGB subgiant branch; MS main sequence; BE blue edge; RE red edge; TO turnuff point (point where stars have evolved off the main sequence); IS instability strip. The data for this figure comes from Demarque et al. (2004), Paunzen et al. (2004), and Aller et al. (1982), while credit to this figure goes to Rose (Brigham Young University, Provo, UT, 2006).

1.5.1 Stellar Evolution and the H-R Diagram

The H-R diagram helped to bring about the current theory of stellar evolution. This theory holds that stars live most of their lives burning hydrogen the way the Sun currently does. However, once these stars begin to run out of fuel to burn, they move into the red giant phase. During the red giant phase stars expand considerably due to a decrease in outward force generated by hydrogen fusion. They also start to fuse helium. Once all their fuel is burned out stars end their lives as white dwarfs,

neutron stars, or black holes. Stars spend most of their lifetime as part of the middle luminosity branch of the H-R diagram. This branch of the H-R diagram is called the main sequence. The giant phase of stellar evolution is associated with the upper, giant branch of the H-R diagram and the dwarf phase of stellar evolution is associated with the lower dwarf branch.

1.6 Variable Stars

Variable stars are stars whose apparent magnitude varies over time. This change in brightness has several causes, including changes in the star's actual luminosity or variations in the amount of light from the star that is blocked from reaching the earth. Variable stars can be classified into two types:

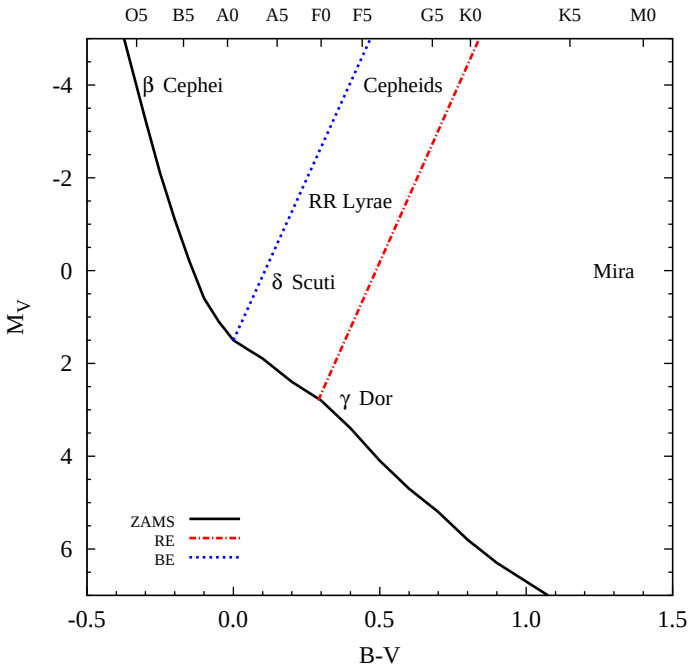

Figure 1.2 Zoomed-in CM diagram that shows the typical locations of pulsating variable stars within the instability strip. Data from the graph comes from Aller et al. (1982) and Paunzen et al. (2004), while credit to this figure goes to Rose (Brigham Young University, Provo, UT, 2006).

intrinsic and extrinsic variables. The inherent brightness of intrinsic variable stars varies over time, whereas the variation in brightness in extrinsic variables is caused by changes in the amount of light that can reach the earth. Intrinsic variable stars have three subdivisions: pulsating variables, eruptive variables, and cataclysmic or explosive variables. Extrinsic variables include rotating stars with sunspots, stars in binary or multiple star systems, and even stars with planets that transit in front of them during their orbits.

Variable stars all lie above the main sequence of the H-R diagram in what is known as the instability strip. The instability strip is depicted as the region between the black dotted lines labeled "IS" in Figure 1.1, as well as in Figure 1.2. The location of variable stars in the instability strip above the main sequences tells us that they are in the giant stage of their stellar evolution. Within the instability strip there are several types of variable stars.

1.6.1 δ Scuti variables

δ Scuti stars reside on the lower portion of the instability strip. They tend to have smaller amplitudes of variation than do RR Lyrae or Cepheid variables. The mechanism of variability in δ Scuti stars is physical pulsation, and they pulsate in both radial and nonradial modes. In other words, the change in shape of these stars as they pulsate is not a function of radius only. δ Scutis have periods of variability between about 30 minutes to 8 hours and photometric amplitudes of less than 1 magnitude.

1.7 Hβ Index

As seen in the above sections discussing the H-R diagram, stellar spectra provide astronomers with a wealth of information. Stellar size, age, temperature, and chemical composition can all be determined using astronomical spectroscopy. This research project involves using spectroscopy to

obtain Hβ indexes of δ Scuti variables.

The Hβ is a measure of the depth of the Hβ spectral line with respect to the continuum or response curve. This measure is obtained as follows: calculating the area above the curve of the absorption line with respect to the continuum over a narrow wavelength range centered on the Hβ spectral line (4861 Å); calculating the area above the absorption line over a wider wavelength range centered on the same spectral line; and taking their difference. Higher indices indicate deeper Hβ absorption lines.

The Hβ index was developed by Bengt Strömgren in the early 1950's (Strömgren 1951). In the same study Strömgren showed that the Hβ index accurately predicts the luminosity and spectral type stars with spectral type B, A, and F. In the mid 1960's Crawford & Mander (1966) updated and standardized the filter sets in the Hβ system. Crawford went on to establish standard stars in the Hβ range as well as perform Hβ photometry on a large number of stars (Crawford et al. 1966),(Crawford 1966). The filters used to calculate Hβ indexes in this research project were taken from Crawford & Mander (1966). See Chapter 3 for more information on the filter sets used. In both Strömgren's and Crawford's work, the Hβ index was determined using photometry rather than spectroscopy; however, with the proper filtering spectroscopy yields accurate results.

1.8 Significance of Hβ Index

The depth of the Hβ spectral line varies in stars. Hβ index is a reliable indicator of stellar temperature. Additionally, since the Hβ index is calculated using relative depths centered on the same wavelength, the index is reddening free, which means it is not necessary to make corrections to the index based on obscuration of light from interstellar dust. Reddening can be present in measurements when differences in magnitude are calculated in two different colors, or magnitudes centered on different wavelengths. One example of a temperature index with reddening is *b-y*. Because the

Hβ index is reddening free and other indices are reddened, plotting the Hβ index against one such as *b-y* can reveal the extent to which certain stars have portions of their radiation blocked through interstellar reddening.

In addition, the Hβ index is an age and metallicity indicator in galaxies and star clusters (Tantalo et al. 1998), (Buzzoni et al. 1994). However, these applications are not explored in this thesis.

1.9 An Additional Note

It should be noted that although the survey of δ Scuti variables includes data from two different telescopes, the research I will present comes exclusively from one of the two telescopes, the 1.2-m telescope. The data reductions and calibration for the 1.85-m telescope are still in progress.

Chapter 2

Observations

In this chapter I describe the data acquisition portion of this research project. This includes the configurations of the telescopes and spectrographs used as well as the details of the survey of known δ Scuti variables that were observed. The data set for this research project comes from a survey of approximately 190 δ Scuti stars in the northern hemisphere, specifically with declinations, or celestial latitudes, above -1° and with magnitudes brighter than 13. The survey aimed to secure observations for as many δ Scuti stars as possible, including stars with published Hβ indices as well as without. A handful of well-known variable stars that are not δ Scuti stars were also observed. Most stars were observed at least two or three times to ensure accuracy of observations. The spectra were obtained at the Dominion Astrophysical Observatory (DAO) in Saanich near Victoria, British Columbia, Canada during eight separate observing runs in 2002 and 2003. Eric Hintz of the BYU Physics and Astronomy department was the primary observer for all observing runs. Refer to Tables 2.1 and 2.2 for a list of all nights during which observations were made. In addition to the Hβ indexes calculated for this research project, rotational velocities for this set of δ Scuti stars have been calculated and published (Bush & Hintz 2008).

Table 2.1. Nights with observations using the 1.2-m telescope.

Night	Hours Observed	No. of Stars Observed	Night	Hours Observed	No. of Stars Observed
March 1/2 2002	12	10	August 9/10 2002	4	5
March 2/3 2002	11	17	August 10/11 2002	9	15
March 3/4 2002	7.5	12	August 11/12 2002	9	13
March 5/6 2002	11	15	August 12/13 2002	9	15
March 6/7 2002	1	2	August 13/14 2002	9	10
June 5/6 2002	2	4	August 14/15 2002	9	18
June 6/7 2002	8	11	August 15/16 2002	7	6
June 7/8 2002	8	10	February 21/22 2003	10	8
June 8/9 2002	2.5	4	February 22/23 2003	3.5	5
June 9/10 2002	6.5	15	February 23/24 2003	12	15
June 10/11 2002	9	15	February 24/25 2003	12	16
June 11/12 2002	6.5	13	February 26/27 2003	12	8

Table 2.2. Nights with observations using the 1.85-m telescope.

Night	Hours Observed	No. of Stars Observed	Night	Hours Observed	No. of Stars Observed
February 26/27 2003	8	15	April 27/28 2004	5	7
March 1/2 2003	3	7	April 28/29 2004	8.5	6
September 12/13 2003	9.5	10	April 29/30 2004	7.5	4
September 14/15 2003	10	12	August 13/14 2004	8	14
September 15/16 2003	2	1	August 15/16 2004	8.5	7
September 16/17 2003	9	5	August 16/17 2004	9	11
April 23/24 2004	9	5	August 17/18 2004	8	6
April 24/25 2004	10	7	August 18/19 2004	8	4
April 25/26 2004	8	7	August 19/20 2004	4	5
April 26/27 2004	6	5			

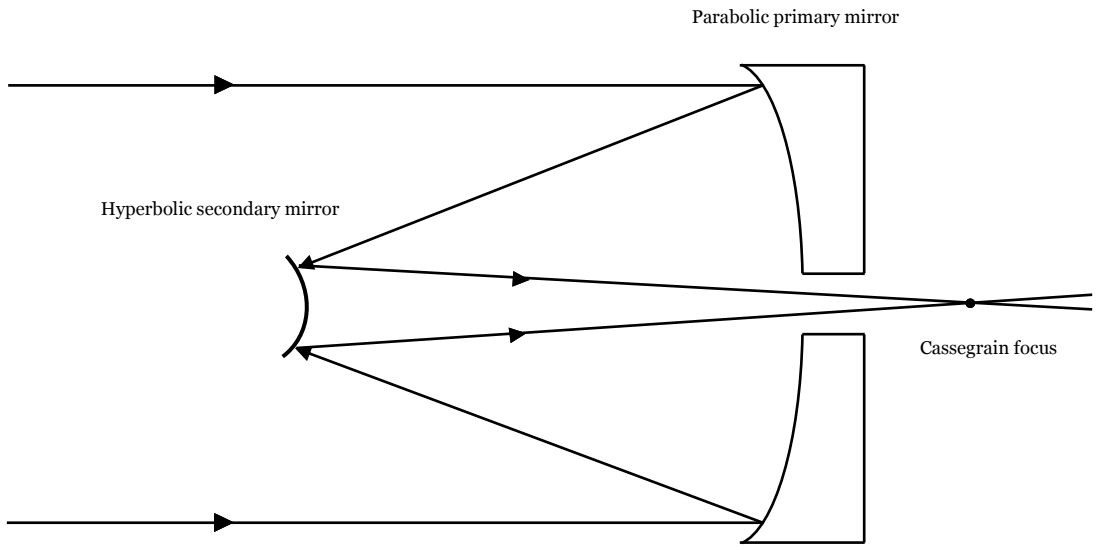

Figure 2.1 Diagram of the path light rays travel in a Cassegrain focus telescope.

2.1 Telescope Configurations

Two DAO telescopes were used to secure observations; one features a Cassegrain focus, and the other a Coudé focus. Both types of telescopes use reflecting mirrors rather than lenses to focus and magnify light. Cassegrain telescopes feature a concave or parabolic primary mirror and a convex or hyperbolic secondary mirror with a small hole drilled in the middle of the primary mirror. The light is directed in the hole and then to the spectrograph (or CCD for direct imaging). Coudé telesopes feature the same kind of primary and secondary mirror as Cassegrain reflectors, but in place of a hole drilled in the primary mirror to collect the light, a third, smaller mirror is used to reflect the light to the side of the telescope and out to the spectrograph. Refer to Figures 2.1 and 2.2 for schematics of both focus types.

The Coudé telescope has a 1.2 meter (1.2-m) diameter and a focal ratio of $f/30$. The Cassegrain telescope, known as the Plaskett telescope, has a 1.85 (1.85-m) meter diameter and a focal ratio of $f/18$. Two telescopes with differing mirror diameters and focal lengths were used so as to enable

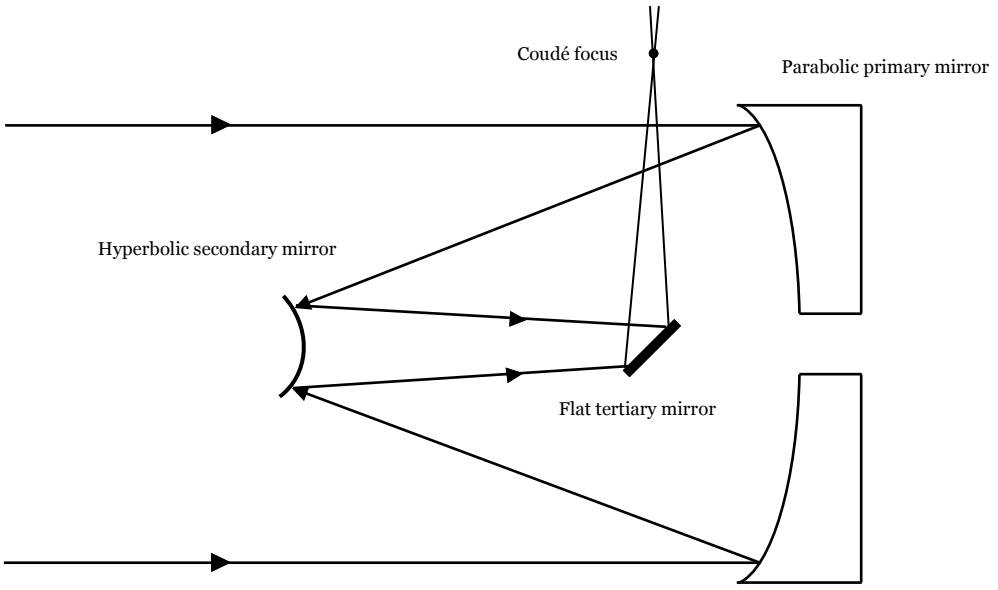

Figure 2.2 Diagram of the path light rays travel in a Coudé focus telescope.

the observation of stars in a large brightness range. The 1.85-m telescope was used to observe the dimmer stars, from roughly 10th to 13th magnitude, and the 1.2-m telescope to observe stars below 10th magnitude. The spectral range in all observations was 3000 to 5000 Å.

2.2 Spectrograph Configurations

The function of a spectrograph is threefold: first, to separate a beam of incoming light into a spectrum of individual light waves, second, to capture the incoming light, and third, to record that light in some manner. In general, a spectrograph design consists of a dispersive device, mirrors to channel the light, and a light detector. There are several kinds of dispersive devices and light detectors. Spectrographs used for astronomical purposes generally utilize a diffraction grating as the dispersive device and a charge-coupled device (CCD) as the light detector.

A diffraction grating consists of a large number of parallel, closely spaced slits. These slits

act as a prism that separates the incoming wave of light into its wavelength components. The spacing of these slits can be changed to manipulate the directions the various beams of dispersed light travel after passing through the grating. A CCD detects and electronically records photons that hit its surface. Various diffraction gratings can be combined with diverse telescope and optical configurations to create a wide range of spectral resolutions. Figure 2.3 shows the typical setup of a spectrograph used for astronomical purposes.

The DAO 1.2-m telescope features a Coudé spectrograph, known as the McKellar spectrograph, while the 1.85-m telescope uses a Cassegrain spectrograph. In a Coudé spectrograph, light coming from the telescopes enters a large room called a Coudé room. This room functions as a large scale spectrograph, where light is collimated, dispersed, and directed to the CCD. The Cassegrain spectrograph follows the setup described in the previous paragraphs with the addition of a field flattener device that corrects optical abberations such as field curvature. The spectrograph configuration for the 1.2-m telescope produces spectra with a dispersion of 0.152 Å per pixel; the 1.85-m telescope yields a spectral dispersion of 0.237 Å per pixel. These dispersions correspond to medium to high resolution spectra which allows for quality observations of the Hβ spectral line.

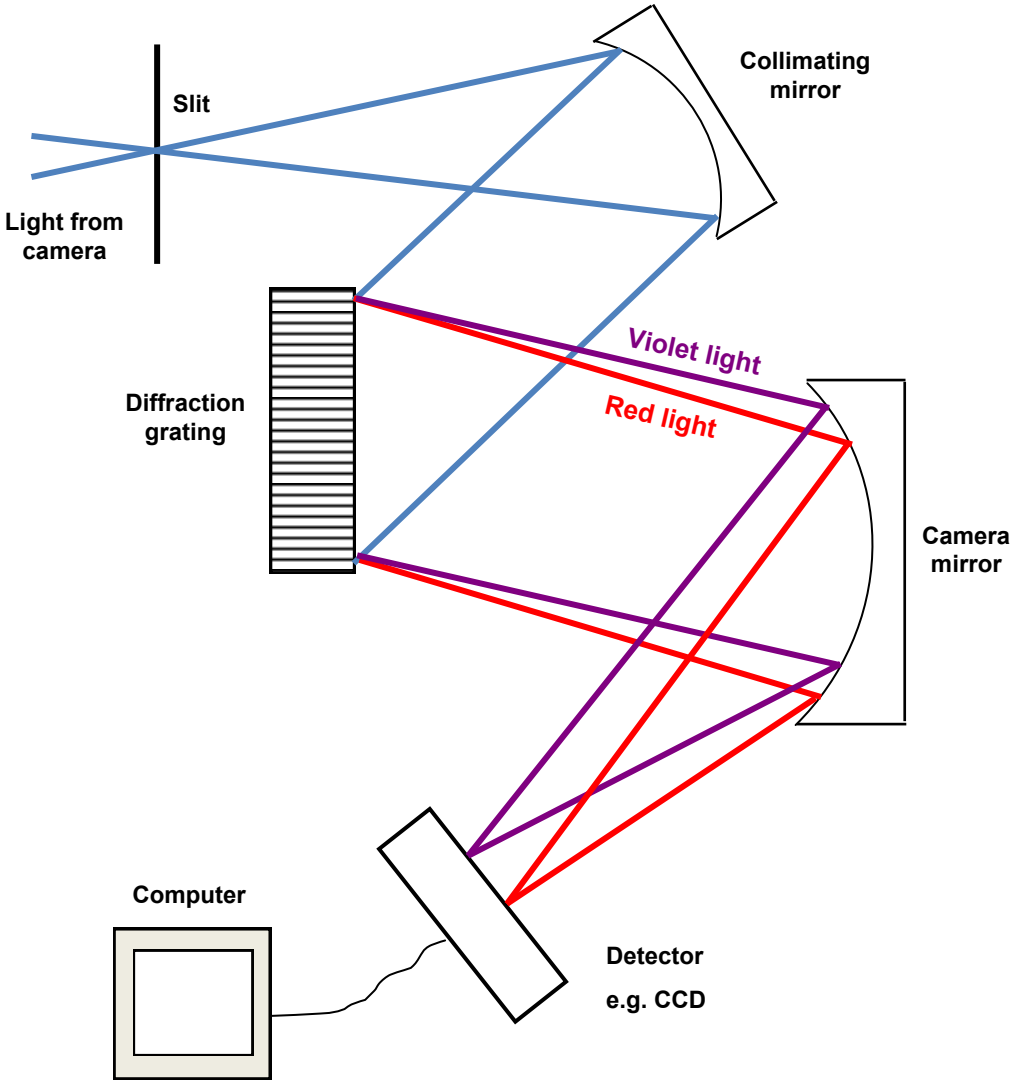

Figure 2.3 General setup of an astronomical spectrograph.

Chapter 3

Spectral Reductions and Calibration

The extraction of Hβ indexes from raw spectral data is a multi-step process. First the data must be processed to reduce noise and correct for imperfections in the CCD. Then a computer program is used to calculate preliminary or instrumental Hβ index values. Finally, a calibration must be performed to produce indexes that are consistent with the standard definition of the Hβ index.

3.1 Standard Calibration frames

To process or reduce spectral data astronomers take different types of CCD spectral images along with the object images. This is done in order to subtract noise in the spectra that arises from different mechanisms as well as to wavelength calibrate the spectra. The calibration images (called frames in observational astronomy) used in this research project are zero frames, flat frames, and arc frames. Zero or bias frames are frames taken with the CCD shutter closed and for an exposure time of 0 seconds. These frames capture the zero or baseline noise that the CCD picks up. Flat fields or frames are images taken of a uniform white surface. These frames measure individual pixel sensitivity to light, dust on the CCD window, internal reflections, and other effects that can distort object spectra. Arc or continuum frames are spectra taken of specific compounds of gas

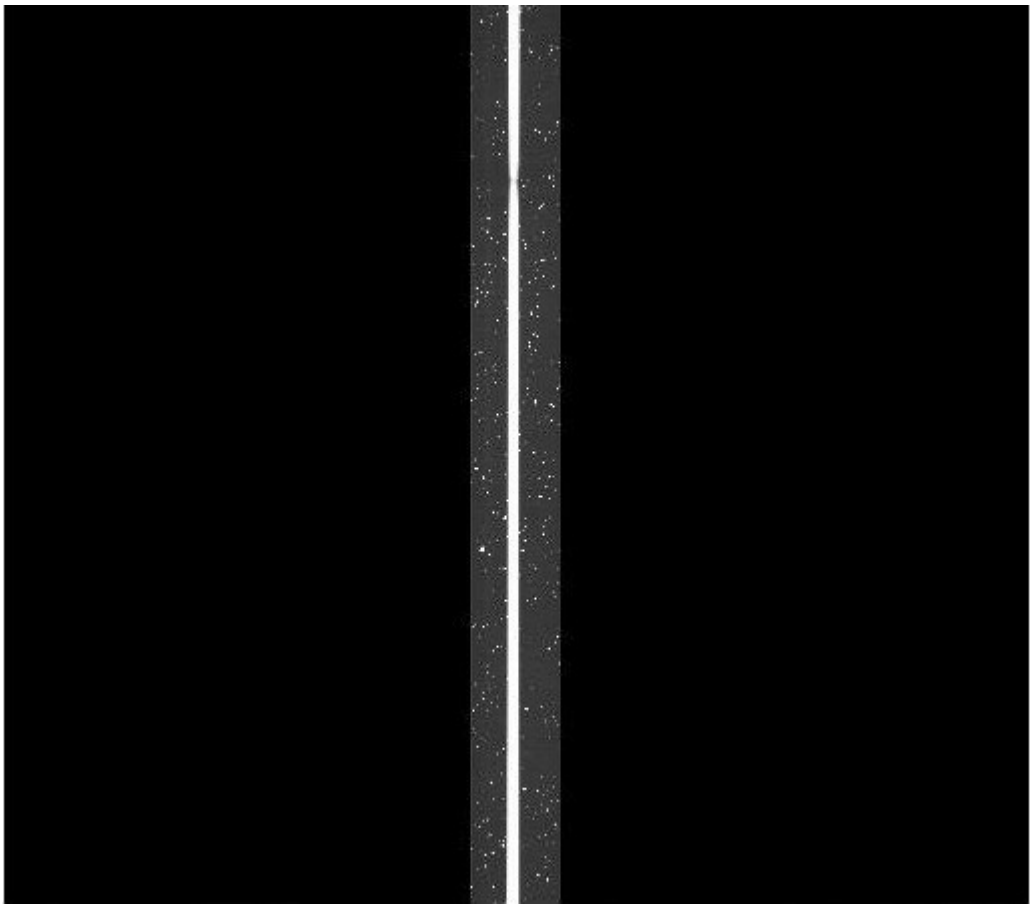

Figure 3.1 CCD image of the spectrum of SAO 16394.

whose spectra are well characterized. Raw object spectra contain information stored as relative intensity per pixel. We convert pixels to wavelength in units of Angstroms by identifying established spectral lines of this gas compound and creating a relation between pixels of the CCD and wavelength. For this research project an iron argon arc lamp was used. At DAO there are two arc lamps available for use: iron argon and thorium argon. Of the two, iron argon features the most distinguishable spectral lines in the wavelength range that contains the Hβ spectral line. Several frames of each type of standard calibration frame were taken for each night of data for this research project. Refer to Figures 3.1 and 3.2 for examples of object frames.

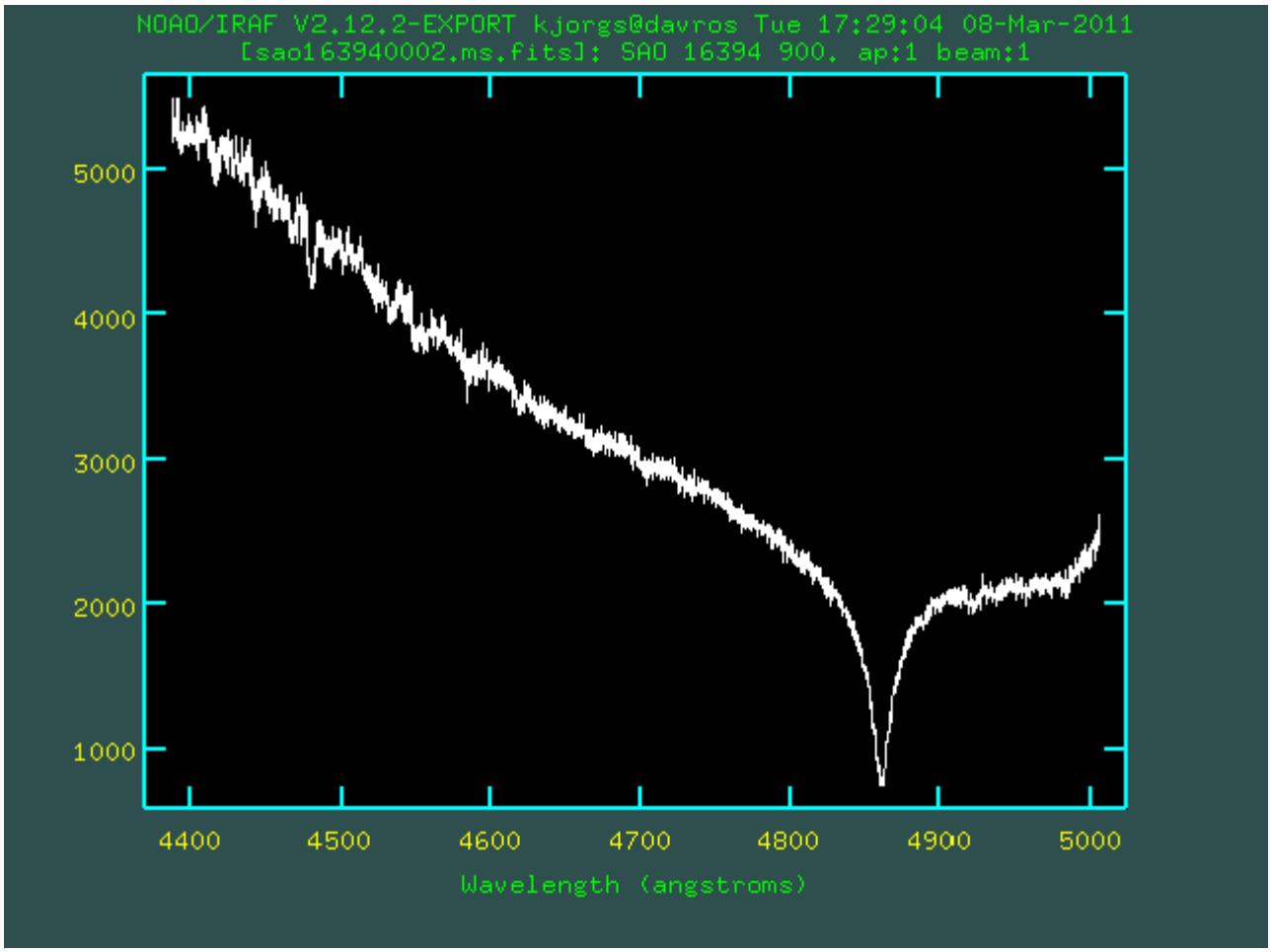

Figure 3.2 IRAF-created image of wavelength calibrated spectra for SAO 16394.

3.2 Reduction Procedures

I reduced the stellar spectra using standard spectral reduction packages in the Image Reduction and Analysis Facility (IRAF), a collection of software geared toward astronomical image reduction. I will now detail my reduction procedures for one night of data. I repeated this process to reduce each night of data.

3.2.1 Eliminating Noise and Distortions

I first took all the bias frames and combined them into a master bias frame by using the IRAF task (or program) *zerocombine*. This task takes the average of all the pixels in the input bias frames. I then used the task *ccdproc* to subtract the master bias frame from all of the flat frames for the night. This eliminates bias noise from the flat frames. I then used *flatcombine* to combine all the flat frames into a master flat in a similar process as *zerocombine*. As seen in Figure 3.1, only a small portion of what the CCD detects actually contains signal. I used the IRAF task *apflatten* to define an aperture where that signal was and set the flat field equal to zero for the rest of the CCD. This task creates a new master flat. Once the master flat and bias frames were ready, I used *ccdproc* again to subtract the bias frame from the object spectra and divide the spectra by the flat frame. This normalizes the object frame and eliminates distortions in the spectra caused by differing pixel response to light.

3.2.2 Wavelength Calibration

Once the noise and distortions were eliminated from my object spectral frames, I then ran the IRAF task *doslit* to define the apertures of the spectra and to wavelength calibrate them. The first part of *doslit* involves interactively defining the aperture of the spectrum or being processed. In the next part, emission lines are interactively identified on frames taken of an arc lamp (in this case iron argon) using an atlas of spectral lines and their associated wavelengths. An example of a spectral atlas, sans a list of wavelengths of the lines, can be seen in Figure 3.3. The task then automatically runs a least squares fit to create a relation between pixel number and wavelength and then applies it to the spectrum. Generally, there are two arc frames taken for each set of data taken at one point in the sky. This ensures the most accurate wavelength calibration for each spectrum. Once I finished running *doslit*, the spectra were ready to produce scientific quality data.

Figure 3.3 Spectral atlas of iron argon. In this plot 15 spectral lines are identified. Credit for this atlas goes to Willmarth (Accessed April 13, 2011).

3.3 Hβ Index Calculation

After the spectra were reduced I ran the IRAF task *sbands* that calculates the Hβ index. This task takes spectra and measures the flux in specific bandpasses using specified filter functions. For the Hβ index, two bandpasses are used: a narrow bandpass 66 Å wide, with a full-width at half maximum (FWHM) of about 30 Å, and a wide bandpass 388 Å wide with a FWHM of 150 Å. Both have a central wavelength of 4861 Å. The filters were approximated from Crawford & Mander (1966); refer to Figure 3.4 for the transmission curves of the filters. The flux in each bandpass is measured by summing each pixel in the bandpass multiplied by the filter response at that pixel. The fluxes of the two bandpasses are converted to magnitudes using the formula

$$m = -2.5 * log(f)$$

where m is magnitude and f is flux in photons per second. The Hβ index is then calculated by taking the difference in the two bandpass magnitudes. This measures the depth of the Hβ absorption line with respect to the continuum.

3.4 Hβ Index Calibration

As discussed above, IRAF contains a program called *sbands* that can calculate the Hβ index. However, the index that IRAF calculates needs to be calibrated to be consistent with the standard Hβ set produced by Crawford & Mander (1966). A calibration is needed because differences in instrumentation used and nightly atmospheric conditions lead to differences in data sets. However, if a set of data is taken correctly, the information extracted from the data such as the Hβ index will

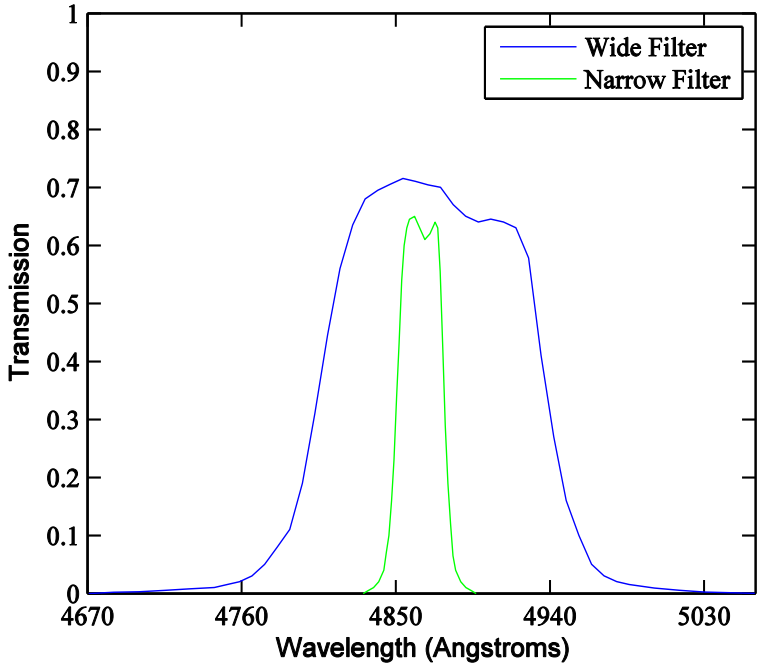

Figure 3.4 Transmission curves for the wide and narrow Hβ filters.

be internally consistent. The instrumental Hβ indexes match the standard Crawford Hβ indexes with the addition of a constant or zero point added to all the indexes in the data set. Hence, the relation between instrumental Hβ indexes and the standard Hβ indexes is linear, with a slope of (or nearly) one and an arbitrary zero point.

As the data set that I used for this research project contains most δ Scuti stars in the northern hemisphere, many of the stars in my data set already have published Hβ index values. I took these values, obtained from Rodríguez et al. (2000) and Hauck & Mermilliod (1998), and once I had the Hβ values produced by *sbands* I plotted the instrumental indexes against the published, standard indexes for these stars. From this I obtained a linear relation between the two. I used this linear relation to calibrate the rest of my data set. I found that I had to find calibration relations for each individual night of observation due to differences in atmospheric conditions during each night. Each night yielded a linear calibration relation with a slope at or close to one, though the

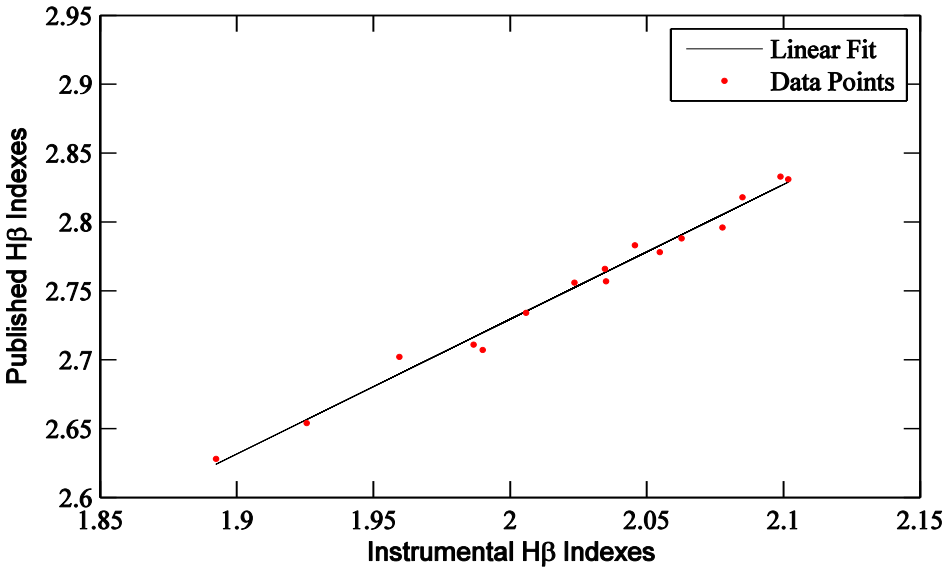

Figure 3.5 Calibration relation for the observing night of February 23/24 2002. The equation for the linear fit is $y = 0.9781x + 0.7733$, where y represents calibrated indexes and x represents instrumental indexes.

zero points all differed. The equation for the linear fit for the various nights of observation looks like $y = mx + b$, where y is the calibrated index, x is the instrumental index, m is slope, which is generally one in this case, and b represents the zero point. Figure 3.5 shows the calibration relation for the observing night of February 23/24, 2002.

As stated earlier, most stars were observed several times. Hence, I obtained multiple Hβ index measurements for most of the stars in the survey. I took the mean of the set of indexes for each star, and then to obtain errors I took the error per mean, described in the following equation:

$$\sigma^2 = \frac{\sum(x-\bar{x})^2}{N(N-1)}.$$

Here σ^2 is the standard deviation or error, x is an individual Hβ index value for a particular star, $\bar{x}$ is the mean index for that star, and N denotes the number of index values for the star.

Chapter 4

Results and Analysis

Tables 1 and 2 show the calibrated Hβ index values, the number of observations, and the uncertainty of the index for each star, as well as *b-y* and spectral type. There were four stars that were only observed once each. This eliminated the option of using the standard method for obtaining uncertainty in the Hβ measurement for these stars. For these stars I used the average or typical error for stars of the same spectral type as their errors. These stars are HD 65934, SAO 140074, V336 Sge, and α Hya. In addition, several stars had higher errors than the rest of the survey. Almost all of these stars are mid-amplitude δ Scuti stars whereas the rest of the survey of stars with unpublished Hβ indexes are low-amplitude δ Scuti stars. Mid-amplitude δ Scutis pulsate on a larger scale, which means that their magnitudes change more significantly as well as their temperatures. Thus their Hβ indexes will vary noticeably.

4.1 Hβ and *b-y*

Once the Hβ indexes were obtained for the given set of stars, I plotted the stars with published *b-y* values against their Hβ index values. I obtained the b-y values from Rodríguez et al. (2000) and also Hauck & Mermilliod (1998). The motivation behind plotting these two values against

Table 4.1. Calibrated Hβ indexes of δ Scuti stars.

Star	No. of Observations	Hβ Index	Error	Published *b-y*	Spectral Type
AD Ari	10	2.811	0.004	0.191	F0
CN Dra	2	2.703	0.005	0.19	F0
EE Cam	3	2.706	0.003	0.31	F0
EO UMa	15	2.740	0.003	0.181	A7III
FG Vir	2	2.759	0.001	0.16	A5
GG UMa	2	2.651	0.003	0.252	F5
GW Dra	3	2.791	0.007		F2
NN Peg	3	2.716	0.002		F0
NU UMa	3	2.736	0.002		G5
QS Gem	3	2.595	0.005		A3
SAO 140074	1	2.879	0.01	0.06	A2
SAO 43050	2	2.843	0.003		A4V
SAO 55207	3	2.824	0.005	0.129	A0
TU UMi	2	2.606	0.015		F2
V1745 Cyg	2	2.769	0.014		A3V
V2084 Cyg	2	2.784	0.015		A3
V336 Sge	1	2.740	0.003		F0
V350 Peg	3	2.737	0.027	0.229	F2
V360 Cep	2	2.816	0.003		A0
V365 And	2	2.710	0.005	0.257	F0
V377 Cep	2	2.805	0.002	0.18	F0
V383 Vul	2	2.699	0.022	0.205	F3II
V388 Cep	2	2.752	0.005	0.171	A7V
V784 Cas	3	2.710	0.002	0.208	F5II
V830 Her	1	2.956	0.003		F2
V919 Her	3	2.857	0.037		F2
V966 Her	5	2.825	0.025	0.204	F2
V979 Her	2	2.720	0.017		A3
ι Boo	3	2.838	0.008	0.128	A6V

Table 4.2. Calibrated Hβ indexes of non-δ Scuti stars.

Star	No. of Observations	Hβ Index	Error	Published *b-y*	Spectral Type
5 Ser	9	2.639	0.003		F8III
HD 65934	1	2.986	0.002		G8III
HD 66141	3	2.564	0.014	0.769	K2III
α Boo	4	2.575	0.003	0.753	K1.5III
α Hya	3	2.577	0.002		K3II-III
β Gem	5	2.592	0.0009	0.611	K0111B
δ Oph	2	2.596	0.0004		M0.5III
μ CMa	2	2.587	0.002		K3III

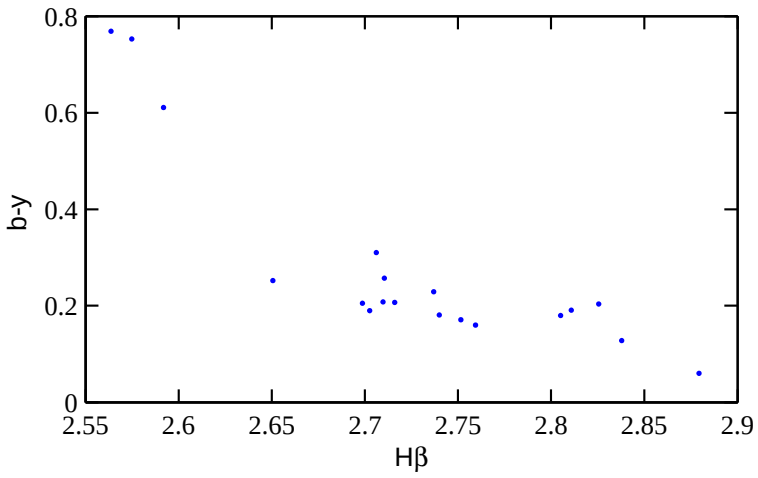

Figure 4.1 Plot of *b-y* vs. Hβ indexes. Hβ indexes at or above 2.65 display a roughly linear relation with the *b-y* color index. Below this the stars' *b-y* and Hβ indexes are not correlated.

each other is that the Hβ index is reddening free, and *b-y* is not reddening free since it involves a color term, and the extinction-dimmed radiation in the blue is not accounted for. Hence, a plot of Hβ vs. *b-y* should reveal the extent to which certain stars are reddened. Figures 4.1 and 4.2 show the resulting plots. Figure 4.1 shows the plot of Hβ vs. *b-y* for stars with known *b-y* values. As

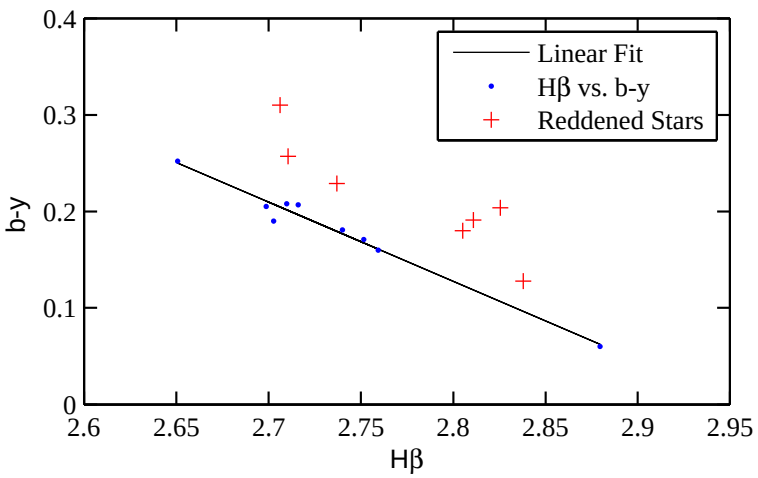

Figure 4.2 The data points corresponding to index values below 2.65 have now been removed. Note the strong linear correlation between Hβ and *b-y* with the exception of the outliers. This indicates that the Hβ index is strongly correlated with the *b-y* index as well as intrinsic stellar temperature.

Figures 4.1 and 4.2 indicate, Hβ indexes at or above 2.65 display a roughly linear relation with *b-y*, while indexes below this are not strongly correlated. Note that the three stars in Figure 4.1 that do not share the correlation of the rest of the stars are all K type stars and not δ Scuti stars. This implies that the Hβ index is only an accurate temperature indicator over certain spectral ranges, which was confirmed by Crawford et al. (1966). This can be attributed to the nature of the strength of the Hβ line as a function of temperature. As discussed in the introduction, the strength of the hydrogen lines in stars peaks at a stellar temperature of about 9900 K, and decreases rapidly for temperatures both above and below this maximum. As seen in Figure 4.2, which is the same plot as in Figure 4.1 with the omission of the three K type stars, we see a linear relation with outliers in the region that features correlation of the two index values. These outliers are most likely reddened by interstellar dust. In conclusion, the calibrated Hβ indexes are publishable, and they display a correct relationship with *b-y*. The outliers in Figure 4.2 are AD Ari, EE Cam, ι Boo, V350 Peg, V365 And, V377 Cep, and V966 Her, and they are most likely reddened stars.

4.2 Future Plans

There are several things that can be done that spring from this research project. First, the reductions and calibration for the data from the 1.85-m telescope need to be completed. Once that has taken place the set of Hβ indices can be put together and published in a scientific journal.

Bibliography

Aller, L. H., et al., eds. 1982, Landolt-Börnstein: Numerical Data and Functional Relationships in Science and Technology - New Series ” Gruppe/Group 6 Astronomy and Astrophysics ” Volume 2 Schaifers/Voigt: Astronomy and Astrophysics / Astronomie und Astrophysik ” Stars and Star Clusters / Sterne und Sternhaufen

Bush, T. C., & Hintz, E. G. 2008, AJ, 136, 1061

Buzzoni, A., Mantegazza, L., & Gariboldi, G. 1994, AJ, 107, 513

Carroll, B. W., & Ostlie, D. A. 2007, An Introduction to Modern Astrophysics, 2nd edn., Vol. 2 (Addison-Wesley)

Crawford, D. L. 1966, in IAU Symposium, Vol. 24, Spectral Classification and Multicolour Photometry, ed. K. Loden, L. O. Loden, & U. Sinnerstad, 170–+

Crawford, D. L., Barnes, J. V., Faure, B. Q., & Golson, J. C. 1966, AJ, 71, 709

Crawford, D. L., & Mander, J. 1966, AJ, 71, 114

Demarque, P., Woo, J. H., Kim, Y. C., & Yi, S. K. 2004, ApJS, 155, 667

Hauck, B., & Mermilliod, M. 1998, A&AS, 129, 431

Paunzen, E., Zwintz, K., Maitzen, H. M., Pintado, O. I., & Rode-Paunzen, M. 2004, A&A, 418, 99

Rodríguez, E., López-González, M. J., & de Coca, P. L. 2000, A&AS, 144, 469

Rose, M. B. Brigham Young University, Provo, UT, 2006, Master's Thesis

Strömgren, B. 1951, AJ, 56, 142

Tantalo, R., Chiosi, C., & Bressan, A. 1998, A&A, 333, 419

Willmarth, D. Accessed April 13, 2011, http://www.noao.edu/kpno/specatlas/fear/fear.html

Index